Accepted Manuscript

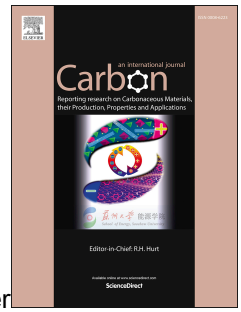

Morphologically disordered pore model for characterization of micro-mesoporous carbons

Piotr Kowalczyk, Piotr A. Gauden, Sylwester Furmaniak, Artur P. Terzyk, Marek Wiśniewski, Anna Ilnicka, Jerzy Łukaszewicz, Andrzej Burian, Jerzy Włoch, Alexander V. Neimark

PII: S0008-6223(16)30828-4

DOI: 10.1016/j.carbon.2016.09.070

Reference: CARBON 11352

To appear in: *Carbon*

Received Date: 8 July 2016

Revised Date: 26 September 2016

Accepted Date: 27 September 2016

Please cite this article as: P. Kowalczyk, P.A. Gauden, S. Furmaniak, A.P. Terzyk, M. Wiśniewski, A. Ilnicka, J. Łukaszewicz, A. Burian, J. Włoch, A.V. Neimark, Morphologically disordered pore model for characterization of micro-mesoporous carbons, *Carbon* (2016), doi: 10.1016/j.carbon.2016.09.070.

Morphologically Disordered Pore Model For Characterization of Micro-Mesoporous Carbons

Piotr Kowalczyk[*1], Piotr A. Gauden[2], Sylwester Furmaniak[2], Artur P. Terzyk[2], Marek Wiśniewski[2], Anna Ilnicka[3], Jerzy Łukaszewicz[3], Andrzej Burian[4,5], Jerzy Włoch[3] and Alexander V. Neimark[6]

[1]School of Engineering and Information Technology, Murdoch University, Murdoch, 6150 Western Australia, Australia

[2]Faculty of Chemistry, Physicochemistry of Carbon Materials Research Group, Nicolaus Copernicus University in Toruń, Gagarin Street 7, 87-100 Toruń, Poland

[3]Faculty of Chemistry, Synthesis and Modification of Carbon Materials Research Group, Nicolaus Copernicus University in Toruń, Gagarin Street 7, 87-100 Toruń , Poland

[4]A. Chelkowski Institute of Physics, University of Silesia, Uniwersytecka Street 4, 40-007 Katowice, Poland

[5]Silesian Center for Education and Interdisciplinary Research, 75 Pułku Piechoty Street, 41-500 Chorzów, Poland

[6]Department of Chemical and Biochemical Engineering, Rutgers, The State University of New Jersey, 98 Brett Road, Piscataway, New Jersey 08854-8058, United States

Corresponding author. Email: P.Kowalczyk@murdoch.edu.au (Piotr Kowalczyk)

Abstract

We present a new morphologically disordered slit-shaped pore (MDSP) model for simulating gas adsorption in micro-mesoporous carbonaceous materials. The MDSP model qualitatively accounts for the inherent roughness of carbon pore walls in accord with the atomistic structural model of LMA10 reference carbon material. The MDSP model is applied to pore size distribution (PSD) calculations from nitrogen adsorption isotherms measured at 77.4 K in the range of pore widths from 0.72 to 40 nm. The MDSP model improves significantly the nitrogen adsorption porosimetry and, being fully atomistic, it is transferable to study various adsorbate-adsorbent systems. Computations of PSD functions for a series of carbonaceous materials, including activated carbon fiber, granular activated carbons, synthetic activated carbons showed that MDSP generates smooth Gaussian-type PSD functions with a well-defined average pore size. Furthermore, PSD functions computed from the MDSP model are free from the artificial gaps in the region of narrow micropores (~1 nm and ~2 nm) predicted from the standard slit-shaped pore models with ideal graphite-like walls. MDSP is not only a complementary model to existing approaches, such as quench-solid density functional theory method, but it paves the way to efficient atomistic simulations of various compounds within morphologically disordered carbon nanopores.

1. Introduction

The morphological structure of nanoporous carbons is usually visualized as an assemble of graphitic planes arranged in a near-parallel fashion embedded in disordered carbon matrix, thus creating a highly porous solid having slit-shaped pores of molecular dimensions [1-4]. One of the experimental justifications for using idealized slit-shaped pores is that the pore walls in activated carbons appear to be graphite basal planes, which present nearly flat surfaces for adsorption [5,6]. Non-local density functional theory (NLDFT) and the grand canonical Monte Carlo simulation (GCMC) have implemented the independent slit-shaped pore model with smooth graphitic walls for pore size analysis of complex micro-mesoporous carbons [7-13]. The use of NLDFT kernels of theoretical nitrogen isotherms (77 K) generated in crystalline graphitic slit-shaped pores has greatly improved the realism of pore size analysis in the micropore region (pore size < 2 nm [14]) compared to the traditional phenomenological methods. However, neglecting the effect of pore wall morphology has prominent drawbacks and, consequently, generates prominent artifacts in the NLDFT pore size distribution (PSD), such as the gap at ca. 1 nm, which is characteristic of many micro-mesoporous carbons [15-19].

Real physicochemical conditions of carbonization and activation processes, used in preparation of micro-mesoporous carbonaceous materials from natural and synthetic precursors, often lead to relatively high energetic heterogeneity of internal surfaces [20-24]. Therefore, it is expected that spatial disorder of carbon atoms within pore walls controls the pore morphology and respectively the surface heterogeneity. Crystallographic defects (e.g. Stone-Wales defects, cluster defects, dislocations, and vacancies), functional groups, and heteroatoms change the curvature of graphene sheets locally or globally [25-30]. Approximation of the complex pore morphology by a simplified pore geometry (e.g., slits, cylinders, spheres, squares, etc.) affects the adsorbate behavior, especially in carbon ultramicropores where the small pore dimensions is ~1-2 times the molecular size of the adsorbate [31,32]. Several approaches were suggested to account for the structural disorder of pore walls in micro-mesoporous carbons. Hybrid reverse Monte Carlo (HRMC) simulation allows for direct reconstruction of the atomistic structural model of nanoporous carbon sample using wide-angle X-ray scattering, helium (296 K) pycnometry and nitrogen (77.4 K) porosimetry data. Although very promising, HRMC is still too complex to be implemented for routine PSD analysis [33-37]. Within the framework of the standard slit-shaped model of nanoporous carbons, a variability of pore walls thickness, surface defects and surface

roughness, energetic heterogeneity, adsorption-induced deformation, wedge-shaped pore model has been introduced [38-43].

The effects of surface heterogeneity have been recently incorporated into pore size analysis within the framework of the quenched solid density functional theory (QSDFT) [44,45]. In this multicomponent DFT method, the solid is modeled using the distribution of solid atoms and the surface heterogeneity is characterized by a single roughness parameter that represents the characteristic width of molecular level surface corrugations. It has been demonstrated that the QSDFT model significantly improves the method of adsorption porosimetry [44,45]. Another approach to account for surface and geometrical heterogeneity of carbon pores is the corrugated graphene model (CGM) , which considers carbon pores as the gaps between corrugated graphene sheets [46,47]. However, neither QSDFT nor CGM approach provides the atomistic structural model of micro-mesoporous carbon, which limits its transferability for computer modeling of other interfacial phenomena, e.g., adsorptive separations, electrochemical energy storage, catalysis, controlled drug delivery, at the atomistic level.

It is important to advance atomistic scale modeling of carbon pores beyond the simple pore geometries to more realistic models. The rational design of pore structure and morphology is crucial to deliver great performance of carbon adsorbents, sieves, catalysts, electrodes, drug carriers, amongst others. Recently, Silvestre-Albero et al. [48] suggested to use the high precision nitrogen adsorption isotherm at 77.4 K measured on a LMA10 carbon material prepared from granular olive stones, as a reference for adsorption studies. The authors argued that LMA10 carbon surface is a good representation of pore walls in disordered micro-mesoporous carbons, and recommended the LMA10 nitrogen adsorption data as a standard for a more accurate pore size analysis of carbonaceous materials [48]. Despite the insights from this experimental work, relatively little is known about the surface structure of LMA10 material at the atomistic level and its impact on the mechanism of physical adsorption. Consequently, how the atomistic-scale morphology of the reference carbon surface affects the PSD analysis of micro-mesoporous carbons remain an open question in fundamental adsorption science. Unfortunately, disordered carbon surfaces, such as LMA10 one, cannot at present be completely characterized experimentally. Methods such as X-ray and neutron scattering, stereo high-resolution transmission electron microscopy (S-HRTEM), scanning transmission electron microscopy (STEM), electron energy loss spectroscopy (EELS), Raman spectroscopy (RS) give valuable partial structural information, but are not yet able to provide an atomistic structural model of disordered carbon surface that

is consistent with the porosimetry measurements [49-53]. It should be also noted that gas adsorption experiment provides averaged pore structure information at different length scales, being quite different from other experimental techniques counted above.

In this work, we present a novel morphologically disordered slit-shaped pore (MDSP) model for characterization of micro-mesoporous carbonaceous materials by nitrogen adsorption. Pore walls in MDSP model are constructed using an atomistic structural model of LMA10 reference material. The rest of the paper is structured as follows. Two-stage optimization approach with experimental and simulation details used for reconstruction of atomistic structural model of LMA10 reference material is described in section 2. We start with the basic idea of the method, followed by the details of the reconstruction of LMA10 carbon surface. Next, we present MDSP model and calculate the kernel of theoretical nitrogen adsorption isotherms for calculations of PSD function from experimental adsorption measurements at 77.4 K. The results of PSD calculations for selected samples of micro-mesoporous carbons are presented in section 3. Final conclusions are given in section 4.

2. Theoretical background, experimental and simulation details

2.1. LMA10 carbon surface: reconstruction methodology

The goal of this work is to develop the atomistic structural model of morphologically disordered slit-shaped carbon pore for characterizations of micro-mesoporous carbons using nitrogen adsorption isotherm measured at 77.4 K. The pore walls in MDSP model are represented by the atomistic structural model of LMA10 reference material, which is reconstructed using a novel heuristic two-step approach. In the first step, we reconstruct the atomistic structural model of highly-graphitized surface using experimental wide-angle X-ray scattering data on Madagascar graphite [54] and HRMC simulation. This graphitic crystal model serves as a base structure for generating atomistic models of micro- and mesopores in disordered carbons. In the second perturbation step, we generate a series of morphologically disordered carbon surfaces by heating and quenching of the graphitic HRMC structure using canonical (NVT) Monte Carlo method. For each generated disordered carbon surface, we determined theoretical nitrogen adsorption isotherm from GCMC simulations. Those theoretical adsorption isotherms are compared against the experimental nitogen adsorption isotherm on LMA10 carbon material to select the most representative atomistic replica of morphologically disordered surface of LMA10 reference material.

2.2. Highly-graphitized carbon surface: wide-angle X-ray scattering experiment

Wide-angle X-ray scattering measurements were performed on Madagascar graphite at ambient temperature on a Rigaku-Denki D/MAX RAPID II-R diffractometer equipped with a rotating anode Ag K_α tube (λ = 0.05608 nm), an incident beam (002) graphite monochromator, and an image plate in the Deby-Scherrer geometry as a two-dimensional detector [55-57]. The pixel size was 100 μm × 100 μm. The investigated sample was placed inside a glass capillary (1.5 mm in diameter and 0.01 mm wall thickens), and measurements were carried out for the sample in the capillary and for the empty capillary, with the intensity for the empty capillary then subtracted. The beam width at the sample was 0.3 mm. The recorded two-dimensional diffraction patterns were integrated over the azimuthal angle to obtain one-dimensional intensity data expressed as a function of the scattering vector Q using suitable software. The scattering vector is defined as $Q = 4\pi \sin(\theta/\lambda)$, where 2θ is the scattering angle and λ is the wavelength. The intensity was then corrected for polarization and absorption and normalized using data processing procedure developed for high-energy X-rays. The structure factor $S(Q) = I(Q)/f^2$ was then determined using the procedure developed for high-energy X-rays and adopted for the Debye-Scherrer cylindrical geometry. I(Q) denotes the corrected intensity normalized to electron units, and f indicates the atomic scattering factor of carbon. The intensity data were then converted to a real space representation in the form of the radial distribution function (RDF) via the sine Fourier transform according to [58]:

$$g(r) = 1 + \frac{1}{2\pi^2 \rho_0 r} \int_0^{Q_{max}} Q[S(Q) - 1]\sin(Qr)dr \quad (1)$$

where ρ_0 = 112 atoms/nm^3 denotes the number density of Madagascar graphite.

2.3. Highly-graphitized carbon surface: hybrid reverse Monte Carlo simulations

We used the HRMC simulation method, the experimental density and radial distribution function measured for Madagascar graphite from WAXS, to reconstruct the atomistic structural model of highly-graphitized surfaces (including thermal effects and possible crystal defects and imperfections) [59,60]. At fixed temperature *T*, we performed Monte Carlo simulation in the canonical ensemble with the transition probability to move from configuration o to n given by:

$$acc(o \to n) = \min\{1, \exp[-\Delta\chi^2/2]\exp[-\beta\Delta U]\} \quad (2)$$

where $\beta = (k_B T)^{-1}$ is the inverse temperature, $\Delta U = U(n) - U(o)$ denotes the difference in potential energy, $\Delta\chi = \chi(n) - \chi(o)$, and χ is given by:

$$\chi = \sum_{i=1}^{M} [g_{theor}(r_i) - g_{\exp}(r_i)]^2 / \sigma_{\exp}^2(r_i) \quad (3)$$

Here, *M* is the number of experimental data points, $\sigma(r)$ is the standard deviations of experimental WAXS data, and $g(r)$ denotes experimental (subscript 'exp') and theoretical (subscript 'theor') RDF.

Theoretical RDF is computed on the fly during the HRMC simulation run from the following expression:

$$g_{theor}(r) = \frac{dN_r V}{4\pi r^2 N dr} \quad (4)$$

where dN_r is the number of carbon atoms in the shell of thickness dr, *N* denotes total number of carbon atoms, and *V* is the volume of the simulation box.

The HRMC algorithm developed by Snook and co-workers [61,62] with experimental RDF measured for Madagascar graphite from WAXS was used for reconstruction of highly-graphitized carbon surface. We start from ground-state electron configuration of carbon atoms in graphite crystal consisting of 9702 carbon atoms in a periodic cubic simulation cell of side length of 4.396 nm (i.e., 2.27 g/cm^3). We assume the error $\sigma(r) = 0.05$ in eq. 3 for each experimental point on RDF. In our HRMC temperature program, we used three stages with linear temperature ramp. In stage 1, all carbon atoms were heated to 5000 K. Next, the temperature was continuously decreased to 800 K. In stage 2, the temperature was dropped from 800 to 500 K. Finally, in stage 3, the temperature was further decreased to 300 K. For temperature quench, we used a total of 10^8 HRMC steps, and each step consisted of attempting displacement of carbon atom. An additional 10^6 HRMC steps at 300 K were performed to compute the theoretical RDF. The surface of Madagascar graphite is similar in nature to the surfaces of other highly-graphitized carbons like Sterling FT carbon black,

which is considered as one of the reference carbons for adsorption studies [8]. The slit pore model with HRMC reconstructed walls is shown on Figure 1 (upper panel). We will further refer to this model as Sterling FT model.

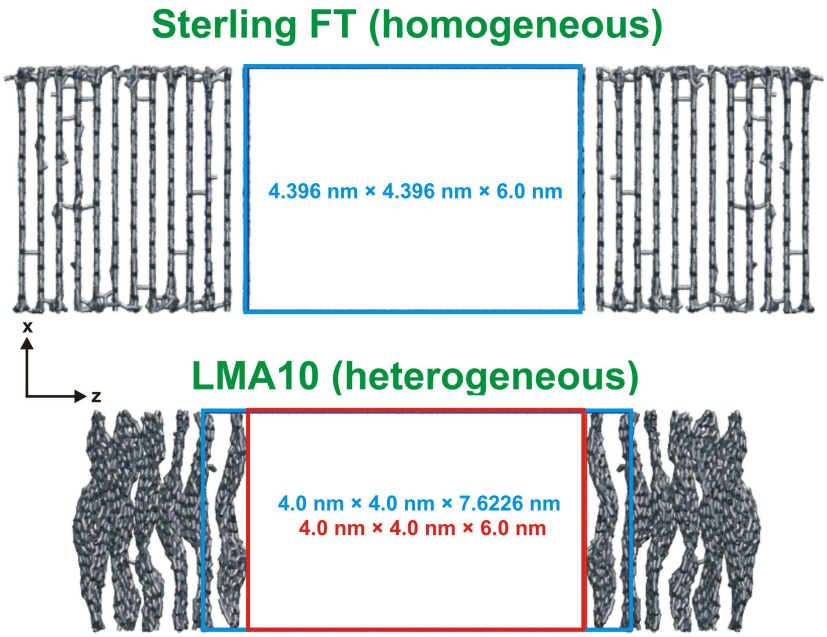

Figure 1. Atomistic structural models used for GCMC simulations of nitrogen adsorption (77.4 K) on highly-graphitized Sterling FT and LMA10 reference carbon surfaces. Note that external surface and intrawall ultramicropores at LMA10 surface are accessible to nitrogen molecules. GCMC sampling regions are displayed by blue rectangular boxes. The smaller red rectangular box refers to a minimal distance between two identical LMA10 carbon walls. The graphics in this figure were created using the VMD program [88].

2.4. LMA10 carbon surface: temperature-quenched Monte Carlo simulations

We assume that LMA10 surface can be generated by the perturbation of the graphitic crystal structure of reconstructed highly-graphitized surface of Madagascar graphite. Thus, we temperature-quench the atomistic model of the base structure using Monte Carlo (MC) method [63,64] with implemented 3-body environment-dependent interaction potential (EDIP) parameterized for carbon-carbon interactions to generate a series of model disordered carbon surfaces [65]. To make the problem computationally efficient, we constructed a smaller graphitic crystal consisting of 3650 carbon atoms by cutting the reconstructed graphitic crystal from Madagascar (bottom panel, Figure 1). In temperature-quench MC simulation, the graphitic crystal was first heated to 5000 K. Next, the temperature was

continuously decreased to 300 K. From the temperature-quench Monte Carlo simulations, we collected 100 atomistic configurations of morphologically disordered carbon surfaces.

2.5. LMA10 and highly-graphitized Sterling FT carbon surfaces: simulated nitrogen adsorption isotherm, isosteric enthalpy and entropy

Adsorption isotherms of nitogen (77.4 K) on LMA10 (heterogeneous) and highly-graphitized Sterling FT (homogenous) carbon surfaces are simulated from the GCMC method [66,67]. Both nitrogen molecules and carbon atoms were modeled by single-site (12,6) Lennard-Jones particles. The fluid-fluid and solid-fluid parameters were taken from the work of Ravikovitch et al. [68]. These parameters correctly reproduce the bulk properties of nitrogen (including: vapor-liquid coexistence, liquid-vapor surface tension, and equation of state) and the adsorption of nitrogen on graphitic carbon surface [68].

For GCMC simulations of nitogen adsorption on highly-graphitized Sterling FT carbon surface, the simulation box of 4.396 × 4.396 × 6.0 nm with periodic boundary conditions and minimum image convention for computing fluid-fluid interactions in x and y directions (upper panel, Figure 1). Two identical carbon walls consisting of 13 graphene sheets separated by a distance of 6.0 nm were kept rigid in GCMC simulations. This set up allowed us to get better estimations of GCMC averages because we simulated nitogen adsorption isotherm on two identical carbon surfaces. The size of the simulation box in direction parallel to pore walls was previously verified in order to eliminate finite size effects [11,68].

For GCMC simulations of nitogen adsorption on morphologically disordered surface of LMA10 material, the simulation box of 4.0 × 4.0 × 7.6226 nm with periodic boundary conditions and minimum image convention for computing fluid-fluid interactions in x and y directions (bottom panel, Figure 1). Two identical LMA10 carbon walls consisting of 6 protruding graphene sheets generated from temperature-quench MC and separated by a minimal distance of 6.0 nm were kept rigid in GCMC simulations. As seen from the snapshot (bottom panel, Figure 1), intrawall ultramicropores at LMA10 surface are generated using temperature-quenched Monte Carlo simulations. We assumed that nitrogen molecules are able to adsorb on both the pore wall surface and also in the intrawall ultramicropores. It is tempting to speculate that nitogen molecules can diffuse from the pore to the intrawall ultramicropores through surface defects; other diffusion paths might be possible as well. In GCMC modeling it is implicitly assumed that intrawall ultramicropores are accessible to

nitogen molecules. Next, we verified this assumption by comparing theoretical GCMC nitogen isotherms with the experimental one measured on LMA10 reference material [48].

For both GCMC simulation setups, fluid-fluid interactions were truncated at 1.81 nm. Interactions of nitogen molecules with all carbon atoms in our molecular models were computed before simulations and stored into a grid. During GCMC simulations, solid-fluid interactions were computed using linear approximation. At each point along the N_2 adsorption isotherm, the simulations were equilibrated using 3×10^7 Monte Carlo steps. The ensemble averages were computed from the additional 5×10^7 Monte Carlo steps. We used the final configuration from the previous adsorption point as a starting configuration for the simulation of the next one.

For nitogen at 77.4 K, the bulk phase was assumed to be ideal gas and the differences between the absolute and Gibbs excess adsorption was neglected. The absolute value of nitogen adsorption per surface area was computed using [66]:

$$n_{abs} = \frac{\langle N \rangle}{2 \cdot S \cdot N_A} \tag{5}$$

where and $\langle ... \rangle$ is the ensemble average, N_A is the Avogadro constant, N is the number of nitogen molecules in the simulation box, and S denotes the surface area of one wall accessible to nitogen molecules. We used the method of Pfeifer et al. [69] to evaluate S.

The isosteric heat of adsorption was computed from the fluctuation theory [66]:

$$q_{st} = RT + \frac{\langle U \rangle \langle N \rangle - \langle UN \rangle}{\langle N^2 \rangle - \langle N \rangle^2} = q_{diff} + RT \tag{6}$$

where U is the configuration energy of the system, T is the temperature, and R denotes the universal gas constant.

To characterize the ordering of nitogen molecules in a course of adsorption we computed the differential entropy of adsorption from the following expression [70-72]:

$$S_{diff} = S_{gas} - \frac{q_{diff}}{T} - R \ln\left(\frac{p}{p_0}\right) + R \tag{7}$$

where S_{gas} (=151.9 J/mol/K) [73] is the molar entropy of the nitogen gas at 77.4 K, $q_{diff} = q_{st} - RT$ is the differential enthalpy of nitogen adsorption, and p denotes the equilibrium pressure of nitogen, and p_0 is the standard-state pressure (=101.325 kPa).

2.6. MDSP model: minimal and average pore size

We implemented the independent slit-shaped carbon pore model with morphologically disordered walls using the atomistic structural model of LMA10 reference carbon material for characterizations of micro-mesoporous carbons by nitrogen adsorption (Figure 2).

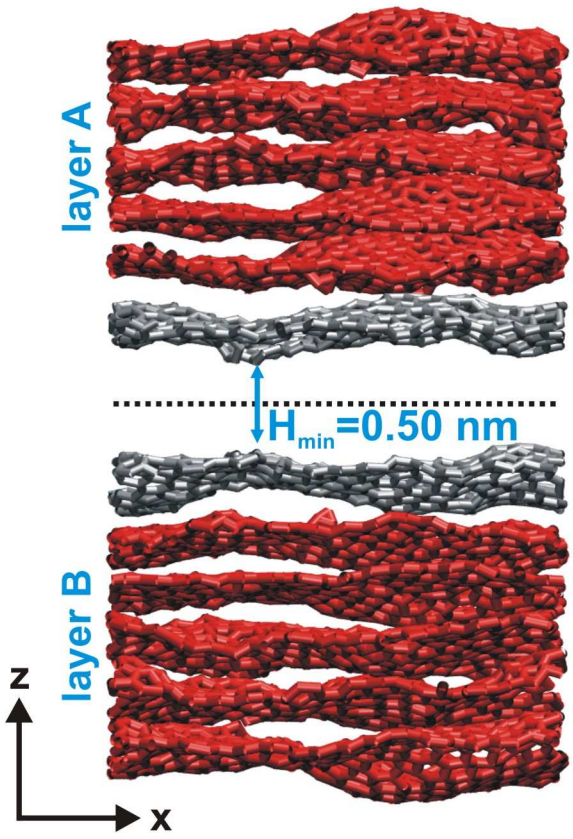

Figure 2. Slit-shaped carbon pore model with morphologically disordered LMA10 walls used for simulations of local nitogen adsorption isotherms at 77.4 K. The middle plane in the pore (i.e. z = 0) is displayed by dotted line. The graphics in this figure were created using the VMD program [88].

Two LMA10 walls, each consisting of 6 protruding graphene-like sheets, periodically imaged in the x and y directions, are placed in the simulation box. These two walls were kept

rigid in GCMC simulations. The accessible pore space is consisting of two regions. The space between the protruding graphene-like sheets is simply called the pore space, and it is characterized by a minimal (H_{min}) and average (H_{avg}) pore width (Figures 2-3). The minimum pore size was varied from 0 to 40 nm. The minimum pore size of H_{min}=0 corresponds to the contact of most protruded from the opposite pore walls carbon atoms. The pore width distributions at selected values of H_{min} are shown in Figure 3. Noteworthy, the average pore widths exceeds the minimum and the average pore width at H_{min}=0 equals 0.72 nm. Intrawall ultramicropores are also accessible to nitrogen molecules. Distributions of the effective pore width (H_{eff}=H-0.34 nm) and the average pore width is computed using Bhattacharya-Gubbins method [74] (BG) (Figure 3 and Figure 1S in supporting information). We considered only the points on the middle plane in the pore (i.e. z=0). The total pore volume corresponds to the volume accessible to the nitrogen hard spheres (collision diameter of 0.3615 nm), and it was determined using combination of BG method and Monte Carlo integration [75].

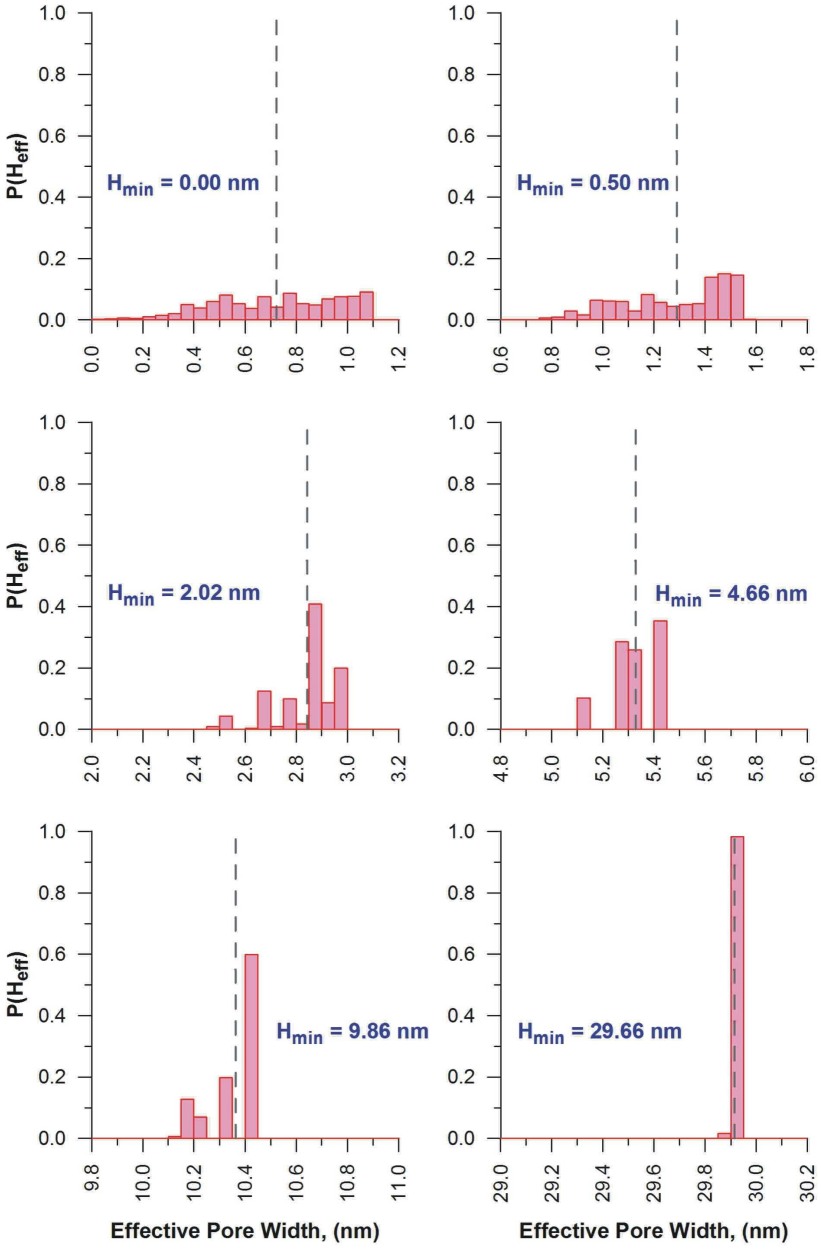

Figure 3. Histograms of the effective pore widths, H_{eff}, detected by the BG method for points on the middle plane in the pore (i.e. z = 0) for selected systems - Figure 2. Dashed lines denote the average pore widths (H_{avg}), 0.72, 1.29, 2.84, 5.33, 10.34 and 29.9 nm, respectively.

The pore size distribution function, $f(H_{avg})$, is determined from the inversion of the discrete form of the integral equation of adsorption [76,77]:

$$N_{\exp}(p) = \sum_i N_{MDSP}(p, H_{avg}) f(H_{avg}) \qquad \text{subject to} \quad f(H_{avg}) \geq 0 \tag{8}$$

where $N_{\exp}(p)$ is the experimental adsorption isotherm interpolated onto the vector of p pressure points, $N_{MDSP}(p, H_{avg})$ denotes a matrix of quantity adsorbed per volume simulated from GCMC with MDSP model. Note that $f(H_{avg})$ is a vector of positive or null values whose terms represent the volume of pore in the sample characterized by an average pore width H_{avg}. The total pore volume of the sample is given by:

$$V_{theor} = \sum_i f(H_{avg}) \tag{9}$$

The numerical solution of a linear discrete ill-posed problem given by eq.8 is not straightforward and special care needs to be taken to obtain physically meaningful solution. In the examples presented below, eq.8 was solved by the second order Tikhonov regularization method with the non-negative least-square algorithm [78,79].

3. Results and discussion

3.1. LMA10 and Sterling FT reference carbon surfaces: microscopic mechanism of nitrogen adsorption

Figure 4(a) presents the HRMC reconstruction of the experimental RDF function measured on Madagascar graphite from WAXS. The agreement between theoretical and experimental RDF is excellent up to measured carbon-carbon distance of 2.0 nm. We note that peaks on experimental and reconstructed RDF functions are finite and broaden by thermal effects and possible crystal defects and imperfections. The theoretical RDF computed for the ground-state electron configuration of carbon atoms in graphite [80] is characterized by a number of sharp peaks. Their positions are in good agreement with experimental RDF measured from WAXS at finite temperature, as shown in Figure 4(b). Figure 4(c) displays HRTEM image of the surface of Sterling FT carbon black, which has been used as a reference material in NLDFT for pore size analysis of micro-mesoporous carbons. The surface of the Sterling FT carbon black is highly-graphitized. Therefore, we expected that nitrogen adsorption on Sterling FT carbon black can be reproduced using structural atomistic model of surface of the Madagascar graphite.

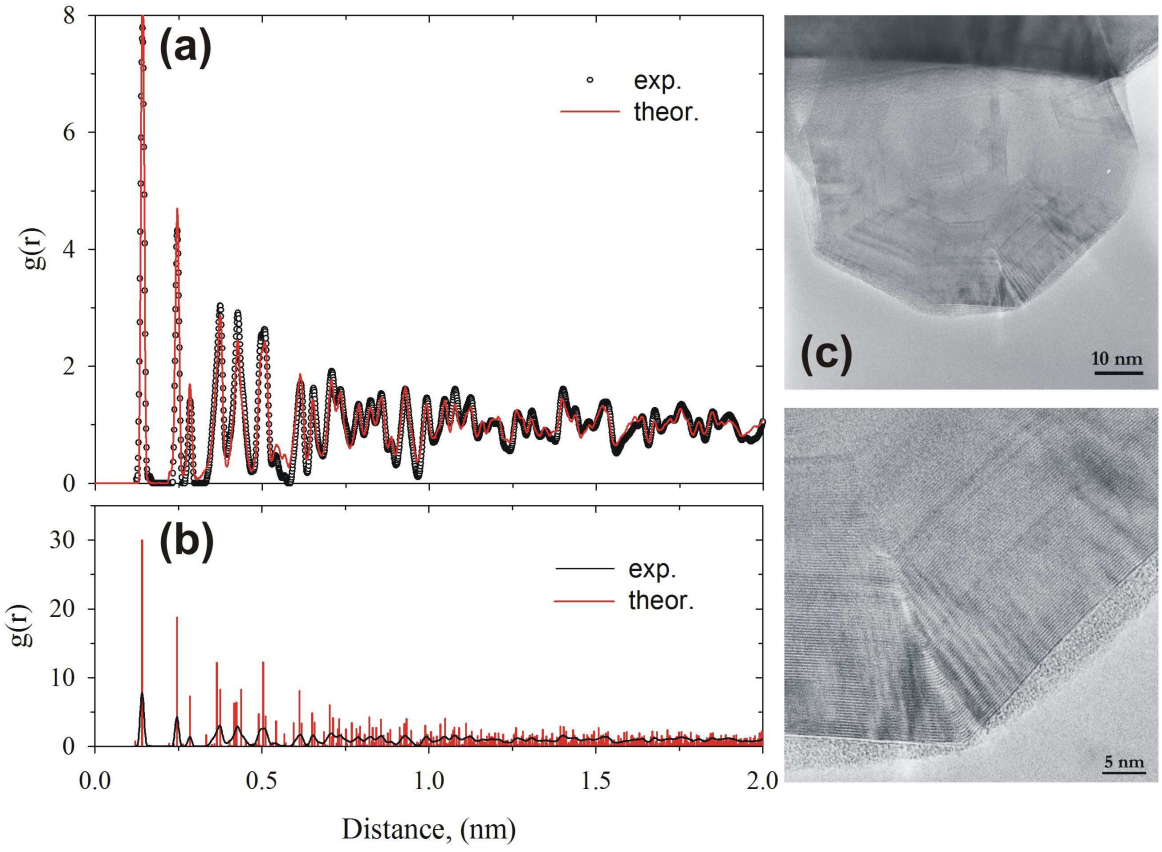

Figure 4. Panel (a) presents the HRMC (theor.) reconstruction of the experimental RDF (exp.) on Madagascar graphite measured from WAXS. The initial RDF generated for ground-state configuration of carbon atoms in graphitic crystal (theor.) [80] is compared with experimental RDF on Madagascar graphite on panel (b). HRTEM images of Sterling FT carbon black are shown in panel (c).

Indeed the experimental nitrogen adsorption isotherm measured on Sterling FT carbon black at 77.4 K is nicely reproduced by the theoretical nitrogen adsorption isotherm simulated from GCMC on the atomistic structural model of highly-graphitized surface of Madagascar graphite (upper panel, Figure 5). The theoretical GCMC nitrogen adsorption isotherm simulated on the most representative morphologically disordered carbon surface at 77.4 K is in very good agreement with the experimental isotherm reported by Silvestre-Albero et al. [48] (bottom panel, Figure 5).

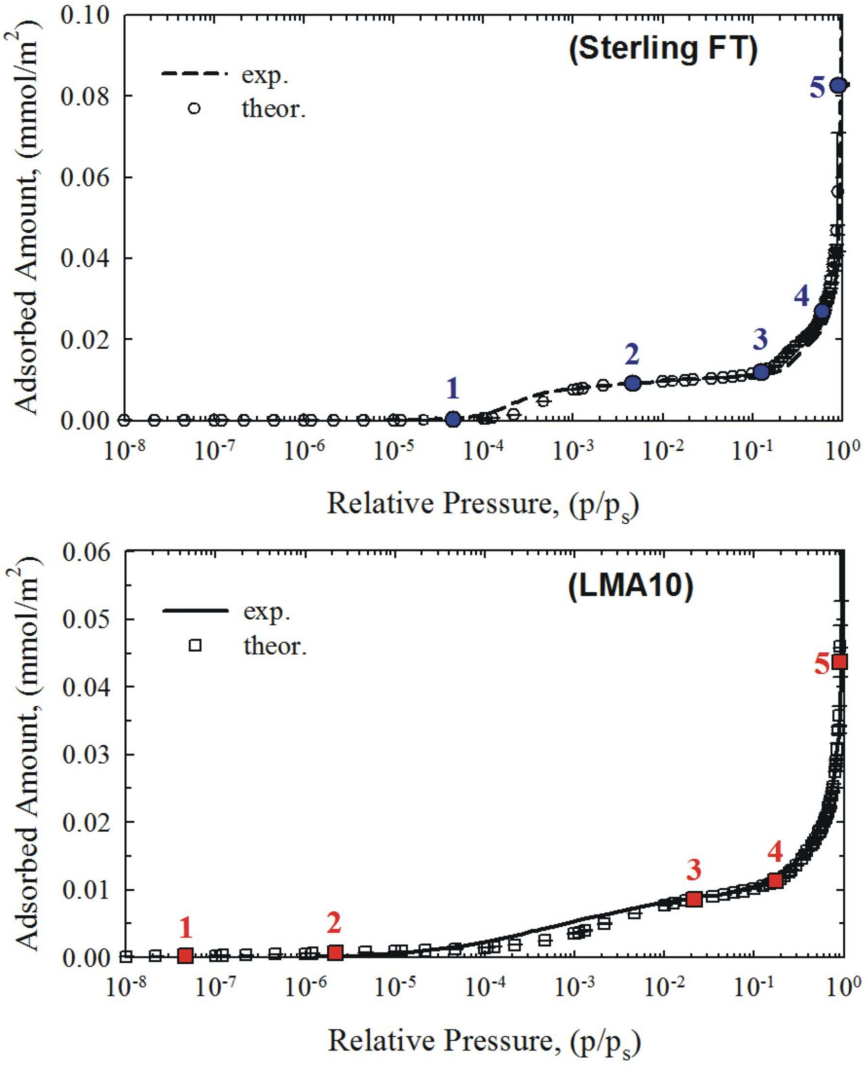

Figure 5. Comparison between the experimental (dashed and solid line) and theoretical nitrogen adsorption isotherms (77.4 K) on Sterling FT carbon black (open circles) and LMA10 carbon material (open squares). The atomistic configurations of nitrogen-carbon interfacial regions at points 1-5 are displayed in Figure 7.

We note, however, that there are significant differences between nitogen adsorption isotherms measured/simulated at 77.4 K on highly-graphitized and morphologically disordered carbon surfaces. Adsorption of nitogen on LMA10 carbon material begins from an extremely low pressure, i.e. 5×10^{-7} p/p_s, and it is increases smoothly without any steps and discontinuities over the entire experimental pressure range (bottom panel, Figure 5). This is a well-known feature of the energetic heterogeneity of the carbon surface, which has been experimentally reported for non-graphitizing carbon blacks [81]. For these materials, the adsorption started on high energetic adsorption centers and proceeds further by gradual filling

of less energetic centers by nitogen molecules. Indeed, the isosteric enthalpy of nitogen adsorption on LMA10 carbon material at low pressures converges to 17.4 kJ/mol (i.e., twice the value of isosteric enthalpy of nitrogen adsorption on Sterling FT carbon black, see upper panel on Figure 6 and Figure 5S in supporting information) and it is smoothly decreasing with further adsorption. Interestingly, we note that the entropy of nitogen adsorption on LMA10 carbon material at 10^{-5} mmol/m^2 is not gas-like, as would be expected for two-dimensional nitogen gas adsorbed on basal plane of graphite (see bottom panel on Figure 6). We found that gas-like entropy of nitogen on LAM10 carbon material corresponds to very low surface coverage of ~2×10^{-7} mmol/m^2 (see Figure 5S in supporting information), indicating the suppression of the local motion of nitrogen molecules adsorbed on LMA10 carbon material at higher surface coverage.

For highly-graphitized sample of Sterling FT carbon black the adsorption of nitogen is negligible up to 5×10^{-4} p/p_s because the basal plane of graphite has no strong adsorption centers. Indeed, the isosteric enthalpy of nitogen adsorption on Sterling FT carbon black at low pressures converges to 8.96 kJ/mol (see Figure 5S in supporting information). Furthermore, we found that nitogen molecules adsorbed on the surface of Sterling FT carbon black behave as two-dimensional gas at low surface coverages, in good agreement with theoretical gas-like entropy of 150 J/mol/K (bottom panel, Figure 6) [73]. Upon further adsorption, nitogen molecules self-assemble into closed-packed monolayer film with theoretical solid-like entropy of 60 J/mol/K. Observed sharp peak on the enthalpy of adsorption and an explicit step on adsorption isotherm at ~10^{-3} p/p_s (see point 2, Figures 5-6) is a further evidence of long-range ordering of nitogen molecules in contact monolayer film. At higher pressures, nitogen adsorption on both reference carbon surfaces followed the mechanism of multilayer formation and grows, as is predicted from Brunauer-Emmett-Teller (BET) theory [82].

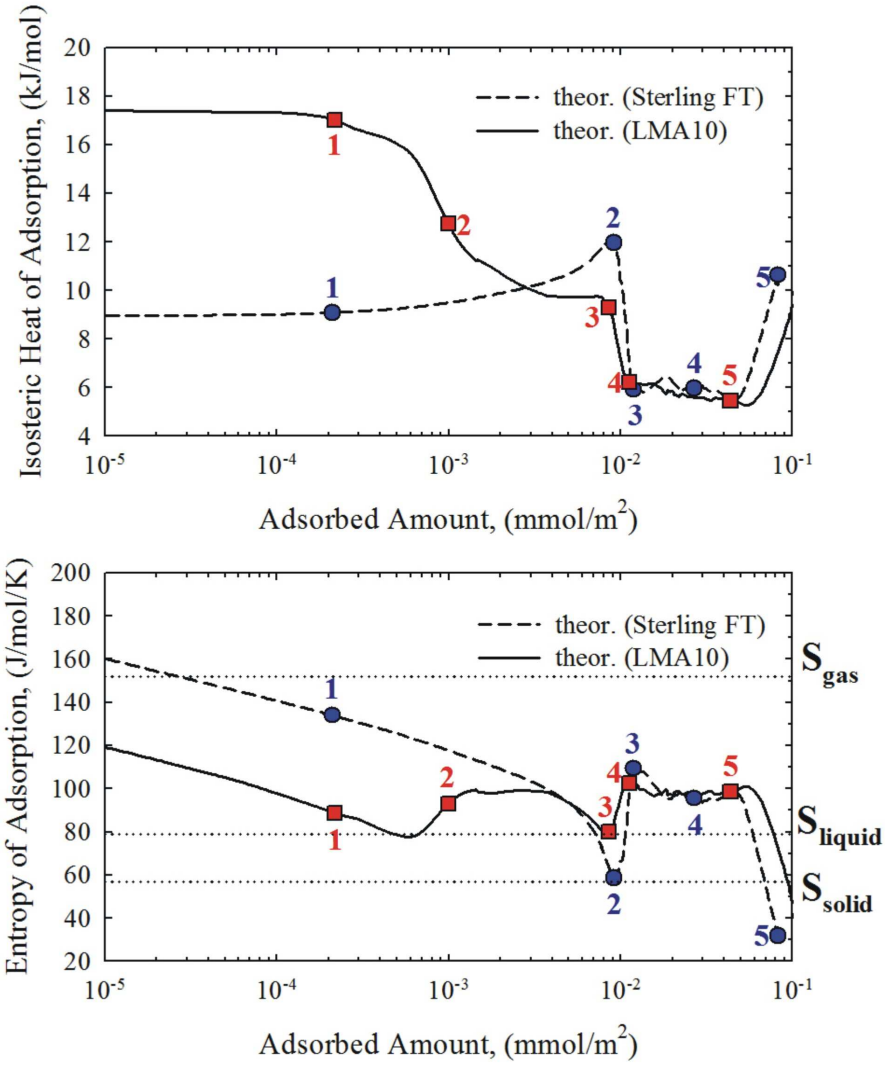

Figure 6. Theoretical isosteric heat (upper panel) and entropy (bottom panel) of nitogen adsorption (77.4 K) on Sterling FT carbon black (open circles) and LMA10 carbon material (open squares). The entropies of gas (S_{gas}), liquid (S_{liquid}) and solid (S_{solid}) N_2 are, respectively: 151.9, 79.133, and 57.03 J/mol/K. The atomistic configurations of nitrogen-carbon interfacial regions at points 1-5 are displayed in Figure 7.

High isosteric heat of nitogen adsorption on LMA10 material computed at low pressures indicates that first adsorbed nitogen molecules experienced some degree of confinement. To make better understanding of theoretical results, equilibrium snapshots of the reconstructed nitogen-carbon interfacial regions for studied reference carbon surfaces are shown in Figure 7.

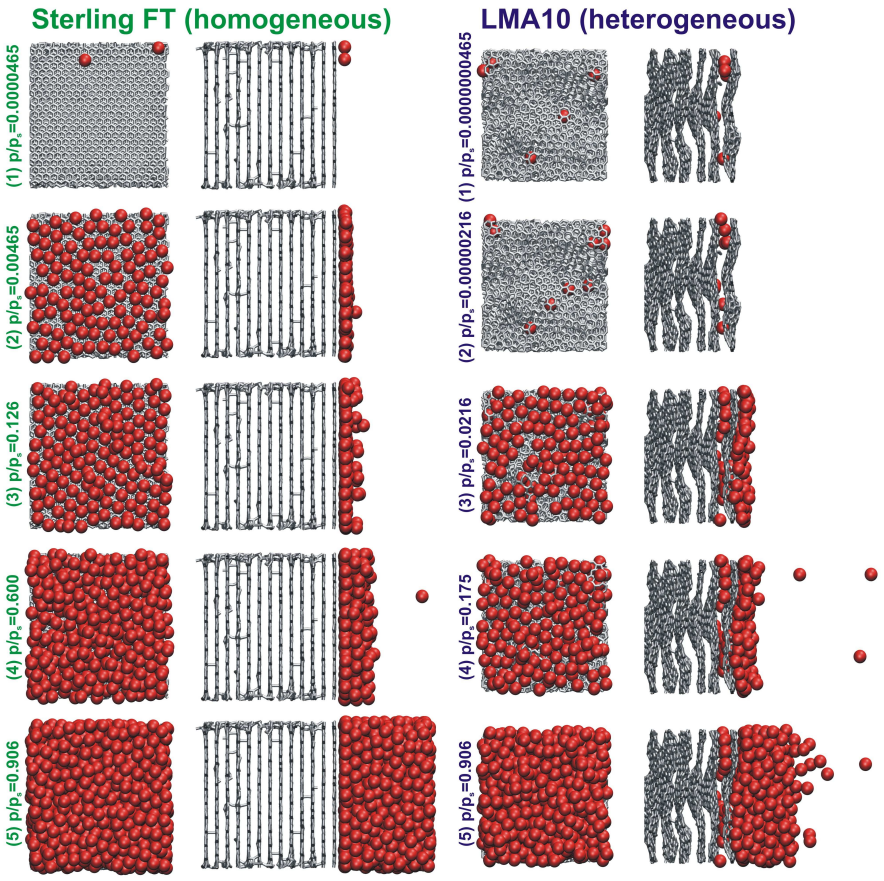

Figure 7. Equilibrium snapshots of nitrogen-carbon interfacial region simulated from GCMC for highly-graphitized Sterling FT carbon black (left panel) and LMA10 carbon material (right panel) at 77.4 K. The relative pressures of coexisting nitrogen gas are displayed on the plot. The graphics in this figure were created using the VMD program [88].

We presented the equilibrium snapshots at one surface only due to symmetry of the slit-shaped pores. It is clear that intrawall ultramicropores on LMA10 carbon surface are generated by the protruding graphene sheets. Narrow carbon ultramicropores with morphologically disordered carbon walls are formed just below the LMA10 external surface. They are responsible for the restriction of translational motion of nitogen molecules in adsorbed phase and high enthalpic effects observed at low pressures (Figure 5 and 6). The presence of structural and energetic disorder around LMA10 carbon surface leads to a smoothing of nitogen-carbon interfacial region and corresponding theoretical nitogen adsorption isotherm. Interestingly and not trivially, our results show that strong confinement can be induced by the atomic-scale roughness of near-surface region of carbon material. Is worth noting the difference between the calculated heats of adsorption for highly graphitized Sterling FT and morphologically disordered LMA10 surfaces given in Figure 6. In the first case, the characteristic non-monotonic behavior with the maximum at point 2 is known in the

literature [83] and can be explained by solidification of the adsorbed monolayer that is confirmed by the calculated entropy. In the second case, the unusual behavior with a pronounced gradual step between points 1 and 3 is explained by the specifics of the adopted model, which allows for adsorption between the corrugated graphene layers. These most energetically favorable sites (q_{st} ~ 17.4 kJ/mol computed at zero coverage, Figure 5S in supporting information) are filled in the beginning of adsorption. Due the surface corrugation, the monolayer (point 3) does not solidify and the further behavior of the heat of adsorption after the monolayer formation is similar to that for Sterling FT sample.

3.2. Local adsorption isotherms and isosteric heats of adsorption

The kernel consisting of 105 GCMC nitrogen adsorption isotherms (77.4 K) has been simulated in MDSP model in the range of average pore widths from 0.72 to 40 nm. All simulated isotherms consisted of 85 points and covered the range of relative pressures, p/p_0, from 10^{-12} to 0.98. Selected excess adsorption and isosteric heat isotherms are presented in Figure 8. Adsorption in micropores of pore size<~1.46 nm is characterized by continuous s-shaped isotherms. At saturation, the density of adsorbed nitrogen in narrow micropores with pore size <~1.0 nm is very high, showing that enhanced surface forces are responsible for solidification and compression of adsorbed nitrogen fluid. In wider micropores of pore size ~> 1.46 nm and mesopores, the isotherms develop discontinues step that corresponds to the first-order capillary condensation from the adsorbed films to the pore filling. We note that the formation and growth of the adsorbed film is continuous, which is manifested by the smooth isotherm prior to the capillary condensation transition. At saturation, density of nitrogen fluid adsorbed in wider micropores and mesopores approaches ~28.8 mmol/cm^3 (i.e., liquid nitrogen) [73]. Intrawall ultramicropores on LAM10 pore walls are responsible for high values of the isosteric heat of adsorption ~17.8 kJ/mol simulated at low pore loadings (bottom panel, Figure 8). With further adsorption of nitrogen, the isosteric heat is continuously decreasing because progressive saturation of energetic sites with higher adsorption energy. Discontinues steps on isosteric heat is a signature of the first-order capillary condensation in wider micropores and mesopores.

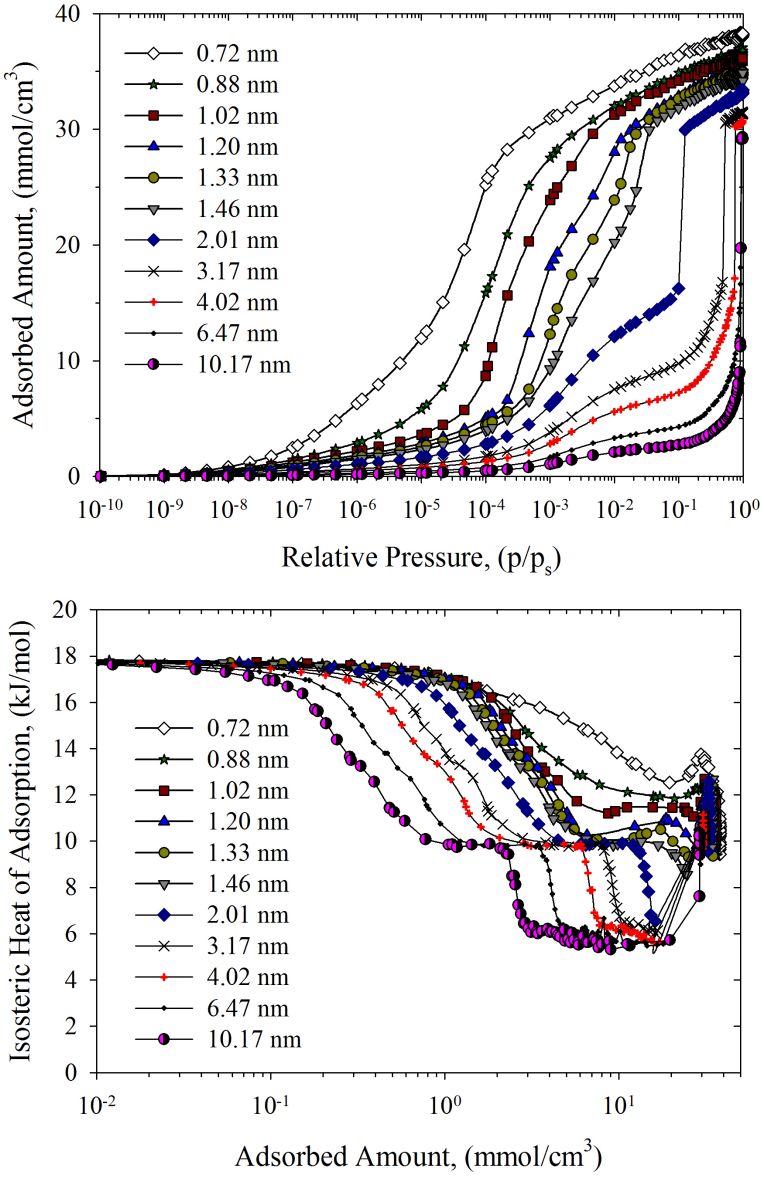

Figure 8. Kernel of selected adsorption isotherms and isosteric heats of nitrogen at 77.4 K in slit-shaped pores with morphologically disordered LMA10 pore walls. The average pore widths are given on the panels.

3.3. Pore size distribution function: application examples

We applied MDSP model to nitrogen (77.4 K) adsorption isotherms measured for spectrum of nanoporous carbonaceous materials, including bituminous coal based activated carbon (Calgon F400) [18,84], charcoal based activated carbon (Norit Row Supra 0.8) [18,84], synthetic activated carbons (prepared from phenolic polymeric precursors), petroleum pitch-based activated carbon fiber (Osaka gas, P25) and chitosan based activated carbons. P25

activated carbon fiber sample was obtained from Prof. Katsumi Kaneko (Shinshu University, Japan) [85]. Micro-mesoporous activated carbons prepared from chitosan precursors were synthetized in our laboratory by Iinicka et al. [86]. High resolution nitrogen adsorption isotherms on chitosan based activated carbons were measured at 77.4 K using the ASAP 2010 MicroPore System (Micromeritics, USA) in the relative pressure range from 1×10^{-6} to 0.99. Before measurement all samples were desorbed in vacuum at 383 K for 3 h [18,84]. A series of nitrogen adsorption isotherms at 77.4 K on synthetic activated carbons prepared from phenolic precursors were obtained from Prof. Mietek Jaroniec (Kent State University, USA) [87].

In Figure 9, we present the pore size calculations for microporous activated carbon fiber P25 using MDSP model and experimental nitrogen isotherm. Figure 9 show that MDSP theoretical isotherm fits the experimental data quite-well over the whole range of measured pressures. We recon some deviations of theoretical isotherm at low pressures, which can be explained by the simplicity of the model. P25 is disordered microporous material with a bimodal structure and high theoretical volume of supermicropores ~1.23 cm^3/g. The majority of supermicropores has average pore widths around ~2-2.2 nm but small fraction of narrow supermicropores around effective pore size ~0.8 nm is clearly visible. The pore size ~2.5 nm provided by the Osaka Gas company is in good agreement with the average pore size computed from the MDSP model.

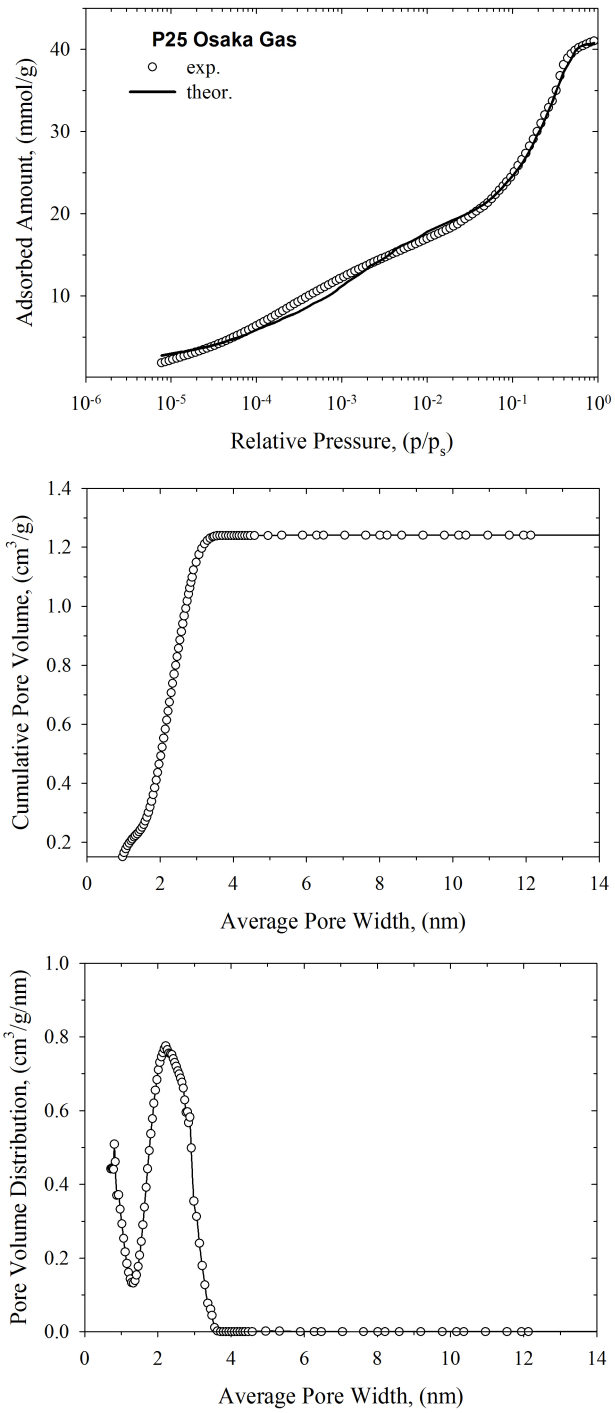

Figure 9. Pore size distribution calculations for pitch based activated carbon fiber P25 (Osaka Gas). Upper panel presents experimental nitrogen isotherm (in semi-logarithmic scale) together with MDSP theoretical isotherm. MDSP cumulative and differential pore volume distributions are presented in middle and bottom panels, respectively.

An instructive example of disordered micro-mesoporous activated carbons is presented in Figure 10. The pore structure of Calgon 400 and Norit Row Supra 0.8 activated carbon is

quite similar. MDSP revels a genuine bimodal structure with micropores < ~2.0 nm and narrow mesopores ~2.0-6.0 nm. We note that, due to the morphological disorder of LMA10 pore walls, the PSDs computed from MPSD model are free from artificial sharp minima such as gaps around ~1 nm, as has been previously reported from NLDFT calculations [11,18,84]. Instead, peaks on PSDs are Gaussian-type with well-defined average pore size. The theoretical adsorption isotherms have some deviations at low pressures, which are explained by the simplicity of MDSP model, which attributes the same level of surface heterogeneity to the pores of different sizes.

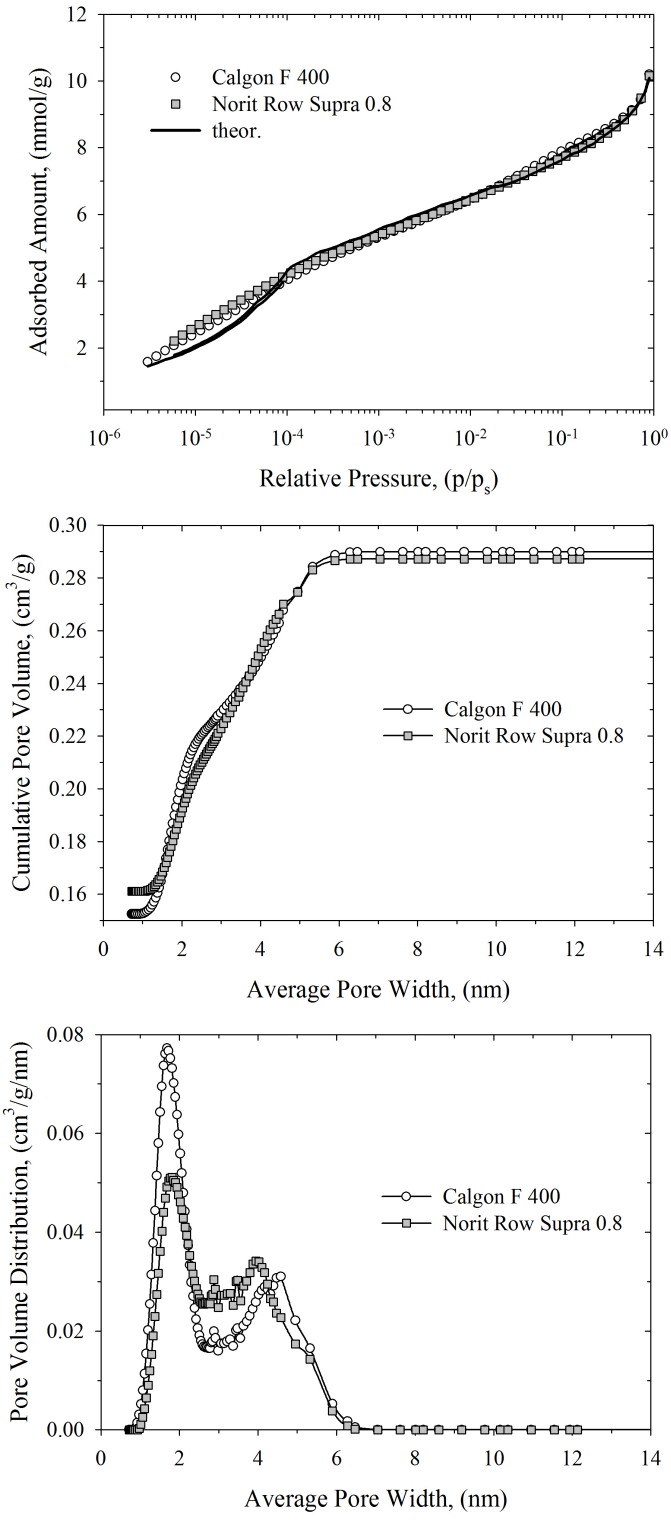

Figure 10. Pore size distribution calculations for granular activated carbon Calgon F 400 and Norit Row Supra 0.8. Upper panel presents experimental nitrogen isotherms (in semi-logarithmic scale) together with MDSP theoretical isotherms. MDSP cumulative and differential pore volume distributions are presented in the middle and bottom panels, respectively.

It is important to investigate the impact of synthesis conditions on the tailored development of micro-mesopore structure. This is demonstrated in Figure 11 and 12, which show PSD calculations for a two series of disordered micro-mesoporous activated carbons, e.g., a series of synthetic activated carbons obtained by Kruk et al. [87], and a series of chitosan based activated carbons synthetized by Iinicka et al. [86].

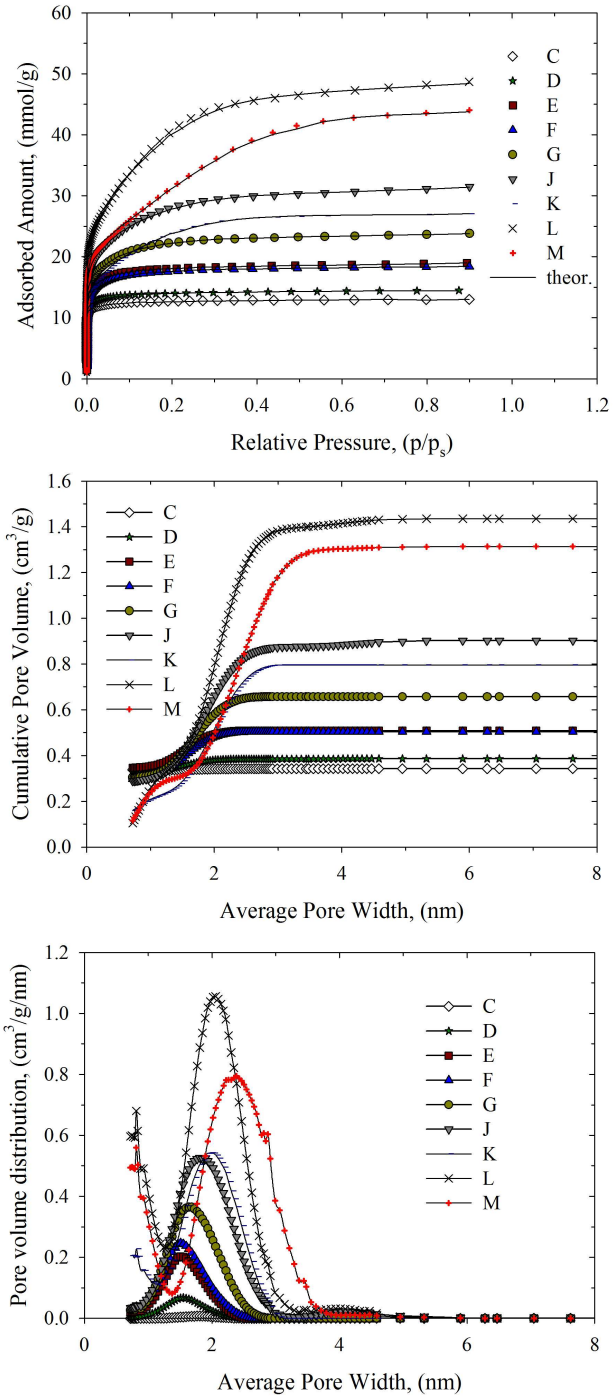

Figure 11. Pore size distribution calculations for a series of synthetic activated carbons synthetized by Kruk et al. [87]. Upper panel presents experimental nitrogen isotherms together with MDSP theoretical isotherms. MDSP cumulative and differential pore volume distributions are presented in the middle and bottom panels, respectively.

The average pore size for synthetic carbons D-J is increases smoothly from ~1.42 nm to a ~1.72 nm (supermicropore range). We note also an increase of dispersion on PSD functions, which can be explained by a longer activation time. On the other hand, samples K-M have a bimodal structure of micro- and narrow mesopores (~2-4 nm). Interestingly, micropores are narrow with the pore size of about ~0.7-0.8 nm (Figure 11). Disordered chitosan based activated carbons are micro-mesoporous solids with a tailored pore size and dispersion on PSD (Figure 12). The carbon samples produced by treatment with phosphoric (V) acid at concentrations 1.34, 2.46, 3.40, 4.21, 4.91, and 5.53 mol/dm^3 were labeled for chitosan as CH_1.34, CH_2.46, CH_3.40, CH_4.21, CH_491, and CH_5.53, respectively. CH_1_34 activated carbon is a strictly microporous solid with an average pore size of ~1.5 nm, whereas CH_8_04 activated carbon is a mesoporous solid with a small contribution from supermicropores (i.e., ~13 % by pore volume). Controlled development of mesoporosity, which was achieved without an expansive and environmentally concerned hard- or soft-templating method, is favorable for the potential applications of these materials in adsorption of larger molecules from solutions, drug delivery systems, and organic-based supercapacitors.

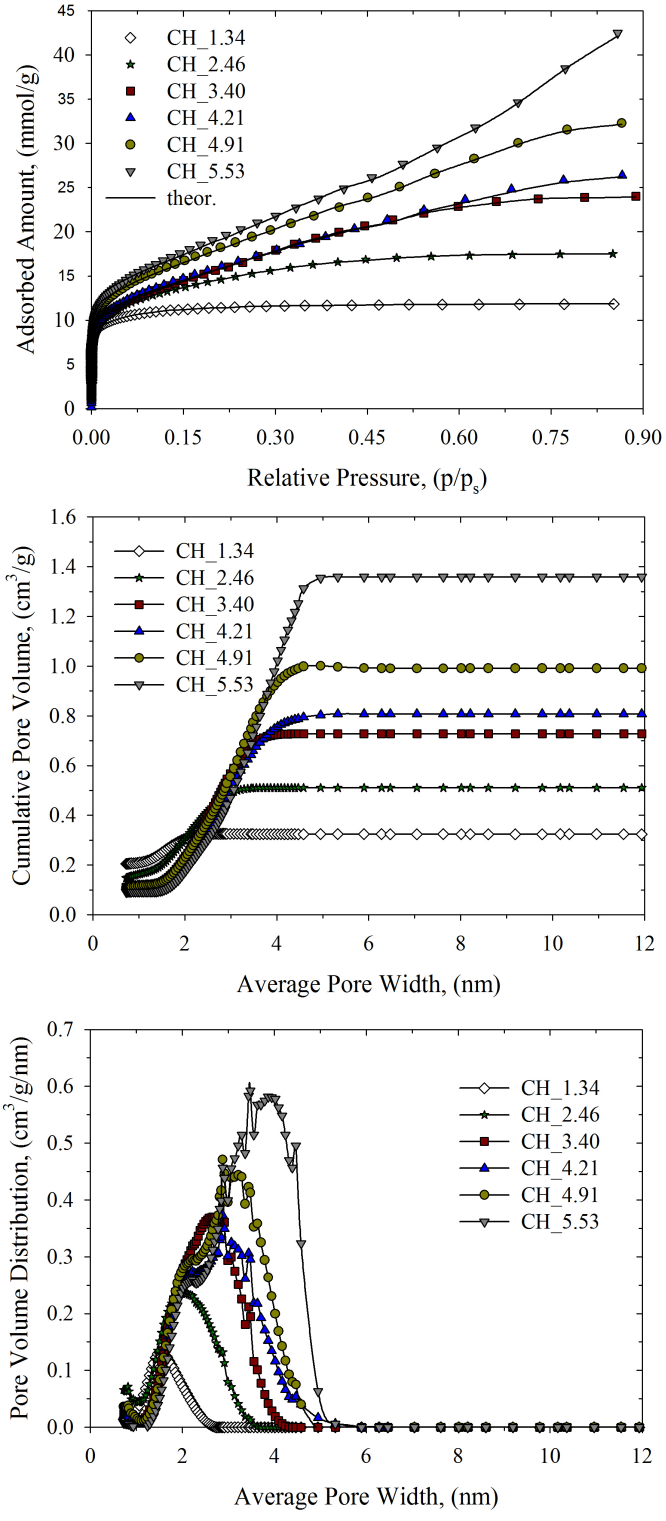

Figure 12. Pore size distribution calculations for a series of chitosan-based activated carbons synthetized by Iinicka et al. [86]. Upper panel presents experimental nitrogen isotherms together with MDSP theoretical isotherms. MDSP cumulative and differential pore volume distributions are presented in the middle and bottom panels, respectively.

4. Conclusions

We develop a morphologically disordered slit-shaped pore model for modeling adsorption and characterization of micro-mesoporous carbonaceous materials. The main feature of MDSP model consists in a qualitative account for the morphological disorder of pore walls in disordered micro-mesoporous carbons using the atomistic structural model of LMA10 reference carbon surface. MDSP model consists of the pore space formed by morphologically disordered graphene layers and intrawall ultramicropores. The energetic heterogeneity of LMA10 reference carbon surface is explained by the presence of intrawall ultramicropores, which existence is an intrinsic structural property of LMA10 surface. Representation of slit-shaped carbon pore walls by morphologically disordered LMA10 surfaces greatly improved the PSD analysis. The MDSP model is demonstrated on various micro-mesoporous carbonaceous materials, including petroleum pitch based activated carbon fiber, bituminous coal and wood based granular activated carbons, polymer and chitosan based microporo-mesoporous activated carbons. It is shown the MDSP model is free of the artificial gaps on PSD functions (~1 nm and ~2 nm) computed from NLDFT and GCMC with smooth graphitic pore walls models. The MDSP model generates smooth Gaussian-type PSD functions with a well-defined average pore size. With additional verification, MDSP may become an alternative model for pore size distribution characterization of porous carbons complementing currently available QSDFT and CGM methods [44-47]. Finally, we demonstrate that the MDSP model can be used for investigations of the tailoring of micro-mesopore structure of activated carbons by synthesis conditions, which is a key element for optimizations of interfacial processes.

It is worth noting that in the proposed MDSP model the LMA10 carbon material was chosen as a reference surface. On principle, it is possible to customize the morphological disorder of carbon pore walls for different classes of carbonaceous materials by choosing relevant reference surfaces. However, further research is needed to shed more light into the relation between the morphological disorder of the surface of the selected reference carbon and the atomistic structure of the pore walls in the disordered carbons to which this model is applied.

Acknowledgments

P.K. acknowledges the financial support from the Office of Research & Development, Murdoch University (startup grant: Nanopore controlled synthetic carbons for interfacial separations and catalysis). P.A.G., A.P.T. and S.F. acknowledge the use of the computer cluster at Poznań Supercomputing and Networking Centre (Poznań, Poland) as well as the Information and Communication Technology Centre of the Nicolaus Copernicus University (Toruń, Poland). P.K. and P.A.G also acknowledge Prof. A. Silvestre-Albero (University of Alicante) for fruitful discussions and comments. A.V.N acknowledges support of Rutgers NSF ERC on Structured Organic Particulate Systems.

Supplementary Data

Supplementary data associated with this article can be found, in the online version.

References

[1] H. Marsh, F. Rodríguez-Reinoso, Activated Carbon, London: Elsevier Ltd., 2006.

[2] S. H. Madani, Ch. Hu, A. Silvestre-Albero, M. J. Biggs, F. Rodríguez-Reinoso, P. Pendleton, Pore size distributions derived from adsorption isotherms, immersion calorimetry, and isosteric heats: A comparative study, Carbon 96 (2016) 1106-1113.

[3] R. C. Bansal, M. Goyal, Activated Carbon Adsorption, Boca Raton: CRC Press, 2005.

[4] M. Inagaki, K. Feiyu, Carbon Materials Science and Engineering – From Fundamentals to Applications, Beijing: Tsinghua University Press, 2006.

[5] J. P. Olivier, Modeling physical adsorption on porous and nanoporous solids using density functional theory, J. Porous Materials 2 (1995) 9-17.

[6] M. Thommes, K. Cychosz, A. V. Neimark, Advanced physical adsorption characterization of nanoporous carbons, in Novel carbon adsorbents, J. M. D. Tascon (Ed.), London: Elsevier Ltd., 2012, pp. 107-145.

[7] Ch. Lastoskie, K. E. Gubbins, N. Quirke, Pore size distribution analysis of microporous carbons: a density functional theory approach, J. Phys. Chem. 97 (1993) 4786-4796.

[8] P.I. Ravikovitch, A. Vishnyakov, R. Russo, A. V. Neimark, Unified approach to pore size characterization of microporous carbonaceous materials from N_2, Ar, and CO_2 adsorption isotherms, Langmuir 16 (2000) 2311-2320.

[9] N. A. Seaton, J. P. R. B. Walton, N. Quirke, A new analysis method for the determination of the pore size distribution of porous carbons from nitrogen adsorption measurements, Carbon 27 (1989) 853-861.

[10] J. Jagiello, M. Thommes, Comparison of DFT characterization methods based on N2, Ar, CO2, and H2 adsorption applied to carbons with various pore size distributions, Carbon 7 (2004) 1227-1232.

[11] P. Kowalczyk, P. A. Gauden, A. P. Terzyk, A. V. Neimark, Screening of carbonaceous nanoporous materials for capture of nerve agents, Phys. Chem. Chem. Phys. 15 (2013) 291-298.

[12] G. M. Davies, N. A. Seaton, V. S. Vassiliadis, Calculation of pore size distributions of activated carbons from adsorption isotherms, Langmuir 15 (1999) 8235-8245.

[13] V. Yu. Gusev, J. A. O'Brien, N. A. Seaton, A self-consistent method for characterization of activated carbons using supercritical adsorption and Grand Canonical Monte Carlo simulations, Langmuir 13 (1997) 2815-2821.

[14] M. Thommes, K. Kaneko, A. V. Neimark, J. P. Olivier, F. Rodriguez-Reinoso, J. Rouquérol et al., Physisorption of gases, with special reference to the evaluation of surface area and pore size distribution (IUPAC Technical Report), Pure Appl. Chem. 87 (2015) 1051–1069.

[15] Y. Gogotsi, R. K. Dash, G. Yushin, G. Laudisio, J. E. Fischer, Tailoring of nanoscale porosity in carbide-derived carbons for hydrogen storage, J. Am. Chem. Soc. 127 (2005) 16006-16007.

[16] P. A. Gauden, P. Kowalczyk, A. P. Terzyk, Toward solving the unstable linear Fredholm equation of the first kind: a new procedure called the adsorption stochastic algorithm (ASA) and its properties, Langmuir 19 (2003) 4253-4268.

[17] J. Chmiola, C. Largeot, P.-L. Taberna, P. Simon, Y. Gogotsi, Monolithic carbide-derived carbon films for micro-supercapacitors, Science 328 (2010) 480-483.

[18] P. Kowalczyk, A. P. Terzyk, P. A. Gauden, R. Leboda, E. Szmechting-Gauden, G. Rychlicki et al., Carbon 41 (2003) 1113-1125.

[19] T. X. Nguyen, S. K. Bhatia, Probing the pore wall structure of nanoporous carbons using adsorption, Langmuir 20 (2004) 3532-3535.

[20] M. Jaroniec, R. K. Gilpin, K. Kaneko, J. Choma, Evaluation of energetic heterogeneity and microporosity of activated carbon fibers on the basis of gas adsorption isotherms, Langmuir 7 (1991) 2719-2722.

[21] D. D. Do, E. A. Ustinov, H. D. Do, Porous texture characterization from gas-solid adsorption, in Adsorption by Carbons, E. J. Bottani and J. M. D. Tascon (Eds.), Oxford: Elsevier Ltd., 2008, pp. 239-271.

[22] H. Jankowska, A. Swiatkowski, J. Choma, Active Carbon, Ney York: Ellis Horwood, 1991.

[23] M. Kruk, M. Jaroniec, J. Choma, Comparative analysis of simple and advanced sorption methods for assessment of microporosity in activated carbons, Carbon 36 (1998) 1447-1458.

[24] J. Choma, M. Jaroniec, Low temperature adsorption of nitrogen on homogenous and heterogeneous nonporous and mesoporous carbonaceous adsorbents, Polish J. Chem. 71 (1997) 380-389.

[25] P. J. Harris, Z. Liu, K. Suenaga, Imaging the atomic structure of activated carbon, J. of Phys.: Condens. Matter 20 (2008) 362201-362206.

[26] L. Zhang, F. Zhang, X. Yang, G. Long, Y. Wu, T. Zhang et al., Porous 3D graphene-abased bulk materials with exceptional high surface area and excellent conductivity for supercapacitors, Sci. Reports 3 (2013) 1408.

[27] A. P. Terzyk, S. Furmaniak, P. A. Gauden, P. J. F. Harris, J. Wloch, P. Kowalczyk, Hyper-parallel tempering Monte Carlo simulations of Ar adsorption in new models of microporous non-graphitizing activate carbon: effect of microporosity, J. of Phys.: Condens. Matter 19 (2007) 406208-406225.

[28] H. Terrones, R. Lv, M. Terrones, M. S. Dresselhaus, The role of defects and doping in 2D graphene sheets and 1D nanoribbons, Rep. Prog. Phys. 75 (2012) 062501-062531.

[29] A. L. Mackay, H. Terrones, Diamond from graphite, Nature 352 (1991), 762.

[30] H. Terrones, M. Terrones, Quasiperiodic icosahedral graphite sheets and high-genus fullerenes with nonpositive Gaussian curvature, Phys. Rev. B 55 (1997) 9969-9974.

[31] P. Kowalczyk, R, Holyst, M. Terrones, H. Terrones, Hydrogen storage in nanoporous carbon materials: myth and facts, Phys. Chem. Chem. Phys. 9 (2007) 1786-1792.

[32] P. Kowalczyk, P. A. Gauden, A. P. Terzyk, S. Furmaniak, P. J. F. Harris, Displacement of methane by coadsorbed carbon dioxide is facilitated in narrow carbon nanopores, J. Phys. Chem. C 116 (2012) 13640-13649.

[33] S. K. Jain, R. J.-M. Pellenq, J. P. Pikunic, K. E. Gubbins, Molecular modelling of porous carbons using hybrid reverse Monte Carlo method, Langmuir 22 (2006) 9942-9948.

[34] J. C. Palmer, J. K Brennan, M. M. Hurley, A. Balboa, K. E. Gubbins, Detailed structural model for activated carbons from molecular simulation, Carbon 47 (2009) 2904-2913.

[35] T. X. Nguyen, N. Cohaut, J.-S. Bae, S. K. Bhatia, New method for atomistic modelling of the microstructure of activated carbons using hybrid reverse Monte Carlo simulation, Langmuir 24 (2008) 7912-7922.

[36] P. Kowalczyk, A. P. Terzyk, P. A. Gauden, S. Furmaniak, M. Wiśniewski, A. Burian et al., Carbon molecular sieves: reconstruction of atomistic structural models with experimental constrains, J. Phys. Chem. C 118 (2014) 12996-13007.

[37] M. Wisniewski, S. Furmaniak, A. P. Terzyk, P. A. Gauden, P. Kowalczyk, Properties of phenol confined in realistic carbon micropore model: experiment and simulation, J. Phys. Chem. C 119 (2015) 19987-19995.

[38] S. K. Bhatia, Density functional theory analysis of the influence of pore wall heterogeneity on adsorption in carbons, Langmuir 18 (2002) 6845-6856.

[39] J. P. Olivier, Improving the models used for calculating the size distribution of micropore volume of activated carbons from adsorption data, Carbon 36 (1998) 1469-1472.

[40] Y. Zeng, P. Phadungbut, D. D. Do, D. Nicholson, Wedge pore model as an alternative to the uniform slit pore model for the determination of pore size distribution in activated carbon, J. Phys. Chem. C 119 (2005) 25853-25859.

[41] E. A. Ustinov, D. D. Do, High-pressure adsorption of supercritical gases on activated carbons: and improved approached based on the density functional theory and the Bender equation of state, Langmuir 19 (2003) 8349-8357.

[42] P. Kowalczyk, Ch. Balzer, G. Reichenauer, A. P. Terzyk, P. A. Gauden, A. V. Neimark, Using *in-situ* adsorption dilatometry for assessment of micropore size distribution in monolithic carbons, Carbon 103 (2016) 263-272.

[43] E. A. Ustinov, D. D. Do, V. B. Fenelonov, Pore size distribution analysis of activated carbons: application of density functional theory using nongraphitized carbon black as a reference system, Carbon 44 (2006) 653-663.

[44] A. V. Neimark, Y. Lin, P. I. Ravikovitch, M. Thommes, Quenched solid density functional theory and pore size analysis of micro-mesoporous carbons, Carbon 47 (2009) 1617-1628.

[45] G. Yu. Gor, M. Thommes, K. A. Cychosz, A. V. Neimark, Quenched solid density functional theory method for characterization of mesoporous carbons by nitrogen adsorption, Carbon 50 (2012) 1583-1590.

[46] J. Jagiello, J. P. Olivier, Carbon slit pore model incorporating surface energetical heterogeneity and geometrical corrugation, Adsorption 19 (2013) 777-783.

[47] J. Jagiello, J. P. Olivier, 2D-NLDFT adsorption models for carbon slit-shaped pores with surface energetical heterogeneity and geometrical corrugation, Carbon 55 (2013) 70-80.

[48] A. Silvestre-Albero, J. Silvestre-Albero, M. Martinez-Escandell, R. Futamura, T. Itoh, K. Ohmo et al., Non-porous reference carbon for N_2 (77.4K) and Ar (87.3K) adsorption, Carbon 66 (2014) 699-704.

[49] K. Kaneko, Determination of pore size and pore size distribution. 1. Adsorbents and catalysts, J. Membrane Sci. 96 (1994) 59-89.

[50] J. Guo, J. R. Morris, Y. Ihm, C. I. Contescu, N. C. Gallego, G. Duscher et al., Topological defects: origin of nanopores and enhanced adsorption performance in nanoporous carbon, Small 21 (2012) 3283-3288.

[51] L. Hawelek, A. Brodka, J. C. Dore, V. Honkimaki, A. Burian, The atomic scale structure of CXV carbon: wide-angle X-ray scattering and modelling studies, J. Phys.: Condens. Matter 25 (2013) 454203-1-7.

[52] Y. Huang, F. S. Cannon, J. K. Watson, B. Reznik, J. P. Mathews, Carbon 83 (2015) 1-14.

[53] C. Hu, S. Sedghi, A. Silvestre-Albero, G. G. Anderson, A. Sharma, P. Pendleton et al., Raman spectroscopy study of the transformation of the carbonaceous skeleton of a polymer-based nanoporous carbon along the thermal annealing pathway, Carbon 85 (2014) 147-158.

[54] S. Wang, F. Tristan, D. Minami, T. Fujimori, R. Cruz-Silva, M. Terrones et al., Activation routes for high surface area graphene monoliths from graphene oxide colloids, Carbon 76 (2014) 220-231.

[55] A. Burian, A. Ratuszna, J. C. Dore, S. W. Howells, Radial distribution function analysis of the structure of activated carbons, Carbon 36 (1998), 1613-1621.

[56] N. Woznicka, L. Hawelek, H. E. Fisher, I. Bobrinetskiy, A. Burian, The atomic scale structure of graphene powder studied by neutron and X-ray diffraction, J. Appl. Cryst. 48 (2015) 1429-1436.

[57] L. Hawelek, A. Brodka, J. C. Dore, A. C. Hannon, S. Iijima, M. Yudasaka et al., Structural modeling of dahlia-type single-walled carbon nanohorn aggregates by molecular dynamics, J. Phys. Chem. B 117 (2013) 9057-9061.

[58] L. Hawelek, J. Koloczek, A. Brodka, J. C. Dore, V. Honkimaki, Y. Ando, Wide-angle X-ray scattering as a quality test for carbon nanotubes, Diamond Relat. Mater. 29 (2012) 18-22.

[59] T. C. Petersen, I. K. Snook, I. Yarovsky, D. G. McCulloch, B. O'Malley, Curved-surface

atomic modeling of nanoporous carbon, J. Phys. Chem. C 111 (2007) 802-812.

[60] A. H. Farmahini, S. K. Bhatia, Hybrid Reverse Monte Carlo simulation of amorphous carbon: distinguishing between competing structures obtained using different modeling protocols, Carbon 83 (2015) 53-70.

[61] G. Opletal, T. C. Peterson, B. O'Malley, I. K. Snook, D. G. McCulloch, I. Yarovsky, HRMC: Hybrid Reverse Monte Carlo Method with Silicon and Carbon Potentials Comput. Phys. Commun. 178 (2008) 777-787.

[62] G. Opletal, T. C. Peterson, I. K. Snook, S. Russo, P.HRMC_2.0: Hybrid Reverse Monte Carlo Method with Silicon, Carbon and Germanium Potentials Comput. Phys. Commun. 184 (2013) 1946-1957.

[63] S. Furmaniak, A. P. Terzyk, K. Kaneko, P. A. Gauden, P. Kowalczyk, T. Itoh, The first atomistic modelling-aided reproduction of morphologically defective single walled carbon nanohorns, Phys. Chem. Chem. Phys. 15 (2013) 1232-1240.

[64] P. Kowalczyk, A. P. Terzyk, P. A. Gauden, S. Furmaniak, K. Kaneko, Toward in silico modeling of palladium-hydrogen-carbon nanohorn nanocomposites, Phys. Chem. Chem. Phys. 16 (2014) 11763-11769.

[65] N. A. Marks, Generalizing the environment-dependent interaction potential for carbon, Phys. Rev. B 63 (2000) 035401.

[66] D. Nicholson, N. G. Parsonage, Computer simulation and the statistical mechanics of adsorption, London: Academic Press, 1982.

[67] M. P. Allen, D. J. Tildesley, Computer simulation of liquids, Oxford: Clarendon, 1987.

[68] P. I. Ravikovitch, A. Vishnyakov, A. V. Neimark, Density functional theory and molecular simulations of adsorption and phase transitions in nanopores, Phys. Rev. E 64 (2001) 011602.

[69] P. Pfeifer, G. P. Johnston, R. Deshpande, D. M. Smith, A. J. Hurd, Structure analysis of porous solids from preadsorbed films, Langmuir 7 (1991) 2833-2843.

[70] P. A. Gauden, S. Furmaniak, J. Włoch, A. P. Terzyk, W. Zieliński, P. Kowalczyk et al., The influence of geometric heterogeneity of closed carbon nanotube bundles on benzene adsorption from the gaseous phase-Monte Carlo simulations, Adsorption 22 (2016) 639-651.

[71] M. Wisniewski, S. Furmaniak, P. Kowalczyk, K. M. Werengowska, G. Rychlicki, Thermodynamics of benzene adsorption on oxidized carbon nanotubes-experimental and simulation studies, Chem. Phys. Lett. 538 (2012) 93-98.

[72] J. K. Garbacz, G. Rychlicki, A. P. Terzyk, A comparison of isosteric and differential

heats of gas adsorption on microporous active carbons, Adsorpt. Sci. Technol. 11 (1994) 15-29.

[73] K. Nakai, M. Yoshida, J. Sonoda, Y. Nakada, M. Hakuman, H. Naono, High resolution N_2 adsorption isotherms by graphitized carbon black and nongraphitized carbon black - α_s-curves, adsorption enthalpies and entropies, J. Colloid Interface Sci. 351 (2010) 507-514.

[74] S. Bhattacharya, K. E. Gubbins, Fast method for computing pore size distributions of model materials, Langmuir 22 (2006) 7726-7731.

[75] D. P. Landau, K. Binder, A guide to Monte Carlo simulations in statistical physics, Cambridge University Press: Cambridge, 2015.

[76] M. Jaroniec, R. Madey, Physical Adsorption on Heterogeneous Solids, Amsterdam: Elsevier, 1998.

[77] J. Jagiello, Stable numerical solution of the adsorption integral equation using splines, Langmuir 10 (1994) 2778-2785.

[78] A. N. Tikhonov, A. V. Goncharsky, V. V. Stepanov, A. G. Yagola, Numerical Methods for the Solution of Ill-Posed Problems, London: Kluwer Academic Publishers, 1995.

[79] P. H. Hansen, Rank-deficient and discrete ill-posed problems, Philadelphia: SIAM 1992.

[80] L. Pauling, The structure and properties of graphite and boron nitride, Proc. Nati. Acad. Sci. USA. 56 (1966) 1646-1652.

[81] M. Sunaga, T. Ohba, T. Suzuki, H. Kanoh, S. Hagiwara, K. Kaneko, Nanostructure characterization of carbon materials with superwide pressure range adsorption technique with the aid of grand canonical Monte Carlo simulation, J. Phys. Chem. B 108 (2004) 10651-10657.

[82] S. Brunauer, P. H. Emmett, E. Teller, Adsorption of gases in multimolecular layers, J. Am. Chem. Soc. 60 (1938) 309-319.

[83] J. Rouquerol, S. Partyka, F. J. Rouquerol, Calorimetric evidence for a bidimensional phase change in the monolayer of nitrogen or argon adsorbed on graphite at 77 K Chem. Soc., J. Chem. Soc., Faraday Trans. 1 73 (1977) 306-314.

[84] P. A. Gauden, E. Szmechtig-Gauden, G. Rychlicki, S. Duber, J. K. Garbacz, R. Buczkowski, Changes of the porous structure of activated carbons applied in a filter bed pilot operation, J. Coll. Inter. Sci. 295 (2006) 327-347.

[85] K. Kaneko, R. F. Cracknell, D. Nicholson, Nitrogen adsorption in slit pores at ambient temperatures: comparison of simulation and experiment, Langmuir 10 (1994) 4606-4609.

[86] A. Iinicka, P. A. Gauden, A. P. Terzyk, J. P. Lukaszewicz, Nano-structured carbon

matrixes obtained from chitin and chitosan by a novel method, J. Nanosci. Nanotechnol. 15 (2015) 1-9.

[87] M. Kruk, M. Jaroniec, K. P. Gadkaree, Nitrogen adsorption studies of novel synthetic active carbons, J. Coll. Inter. Sci. 192 (1997) 250-256.

[88] W. Humphrey, A. Dalke, K. Schulten, VMD - Visual Molecular Dynamics, J. Mol. Graph. 14 (1996) 33-38.